Rediscovering our Galaxy
Proceedings IAU Symposium No. 334, 2017
C. Chiappini, I. Minchev, E. Starkenburg
& M. Valentini, eds.
© International Astronomical Union 2018
doi:10.1017/S1743921317007542

The IMF in the Galactic Disk and Bulge are Indistinguishable

Christopher Wegg, Ortwin Gerhard and Matthieu Portail

MPI für Extraterrestrische Physik, Giessenbachstrasse, 85748 Garching, Germany.
email: wegg@mpe.mpg.de

Abstract. We have measured the IMF of the inner Galaxy using ~ 3000 OGLE-III microlensing events. Each event's timescale depends on both the lens mass, and the velocities and distances of the lens and source. New dynamical models were used provide the distribution of distances and velocities, and thereby measure the lens mass distribution. Using a power-law or log-normal parameterisation the resultant IMF is indistinguishable from local measurements by Kroupa or Chabrier respectively. The lenses lie in the inner Galaxy where the stars are mostly $\sim 10\,$Gyr old and formed on a fast α-element enhanced timescale thereby constraining IMF variability with the properties of the collapsing gas cloud. Furthermore microlensing measures the stellar mass budget, including dark remnants, to low mass. Stars contribute most of the mass in the inner Galaxy with a low fraction remaining for dark matter. Reconciling this with local dark matter estimates requires a core or shallow cusp in its profile.

Keywords. stars: mass function, Galaxy: bulge, Galaxy: stellar content, Galaxy: structure

1. Introduction

The present day mass function (PDMF) and the initial mass function (IMF) of stars are important throughout astronomy. The PDMF for example is the key ingredient in inferring the stellar masses of galaxies from their light. The IMF is equally important, controlling the PDMF, but also the the enrichment and return of gas to the interstellar medium. Despite the importance of the IMF we have little understanding of how it arises from the physics of the collapsing gas clouds. A variety of methods have been used to measure the PDMF and infer the IMF. The most direct are from nearby star clusters and field stars where star counts make the measurement fairly robust outside the lowest mass brown dwarfs (see e.g. Bastian *et al.* 2010).

There are however suspicions that the IMF could vary with redshift or formation timescale because of, for example, dependence on the temperature and density of the collapsing interstellar gas. There has therefore been a great effort to extend our knowledge of the IMF outside the solar neighbourhood. While results have indicated that the IMF may vary, particularly in massive ellipticals (e.g. van Dokkum & Conroy 2012), a consensus is yet to emerge.

Bulge microlensing offers a unique tool for measuring the mass function in the inner Milky Way (MW), where the majority of stars formed quickly at redshift $z > 1$. A more detailed description of the results summarised here is given in Wegg *et al.* (2017).

2. The IMF in the Inner Galaxy Measured Through Microlensing

Microlensing occurs when a background source star passes in projection within the Einstein radius of a nearer star or stellar remnant and the light from the background star is hence amplified. From each events light curve a characteristic timescale can be

https://doi.org/10.1017/S1743921317007542 Published online by Cambridge University Press

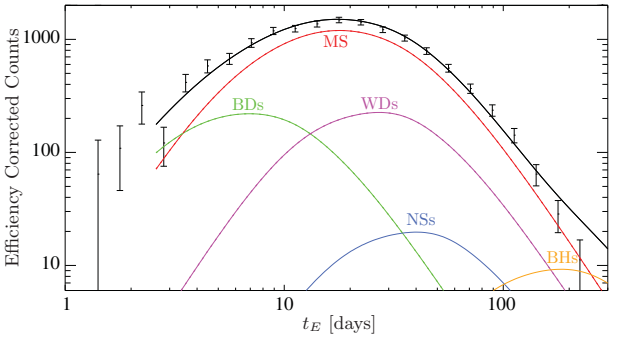

Figure 1. The efficiency-corrected timescale distribution from Wyrzykowski *et al.* (2015) compared to the best fitting power-law IMF with 0% binary fraction. Coloured lines show the contribution to the model from different stellar objects. Adapted from Wegg *et al.* (2017).

measured. This timescale, t_E, is the time for the lens and source to travel 1 Einstein radius in projection: $t_E \equiv R_E/V = \left[4GM_l D_l^2/c^2 \left(D_l^{-1} - D_s^{-1}\right)\right]^{1/2}/V$. It therefore attractively depends mass of the lensing object, M_l. Unfortunately it also depends on the relative motion of the lens and source star, V, and their distances, D_l and D_s. Normally there is insufficient information to infer all these from a microlensing event, and so the lens mass, and the distances and velocities of the lens and source are degenerate. Dynamical models are however able to provide the distribution of distances and velocities, and therefore from the microlensing timescale distribution the lens mass distribution can be measured.

In particular it is straightforward to show from definition of t_E that the timescale distribution arises from the convolution of the square-root weighted lens mass distribution with the timescale distribution predicted by the dynamical model if all lenses were monomass. With a given dynamical model the range of lens mass distributions consistent with the data can therefore be computed.

This method has been used to infer lens mass distributions several times in the literature (e.g. Calchi Novati *et al.* 2008, and references therein). Our work improves on earlier ones in two respects. (*a*) The microlensing sample size is greatly increased: We use the sample of microlensing events provided by Wyrzykowski *et al.* (2015). After removing highly blended events, we use 2861 events with well measured timescales. (*b*) The dynamical model is much improved, being fitted to a wide range of new MW data. We use the dynamical model derived from inner Galaxy data by Portail *et al.* (2017, P17) using the made-to-measure method. In this work an initially barred N-body model was fitted to a wide range of data consisting of: the 3D shape of the Bulge (Wegg & Gerhard 2013), near-infrared star counts Wegg *et al.* (2015), and kinematics from the BRAVA (Kunder *et al.* 2012) and ARGOS (Ness *et al.* 2013) surveys. The reader interested in the more details of the dynamical model is referred to P17.

We consider IMFs of broken power-law form, $dN \propto M^{-\alpha}\, dM$, with slopes $\alpha_{\rm ms}$ in the main sequence region from $0.08M_\odot \leqslant M < 0.5M_\odot$ and $\alpha_{\rm bd}$ in brown dwarf region from $0.01M_\odot \leqslant M < 0.08M_\odot$. We fix the slope above $0.5M_\odot$ to be 2.3, because at these masses the IMF in the bulge is securely measured by HST star counts and is constrained beyond turnoff by chemical evolution models. The resultant best fitting timescale distribution is shown in Fig. 1. We fit the distribution over the range $2\,\text{days} < t_E < 200\,\text{days}$, removing the shortest or longest timescale events since these are the subject of dedicated studies to detect free floating planets and black holes respectively. The model over predicts the number of long timescale events, however we checked that the results are unchanged if we restrict the fit to $t_E < 100\,\text{days}$. The very recent OGLE-IV sample of events from Mróz

https://doi.org/10.1017/S1743921317007542 Published online by Cambridge University Press

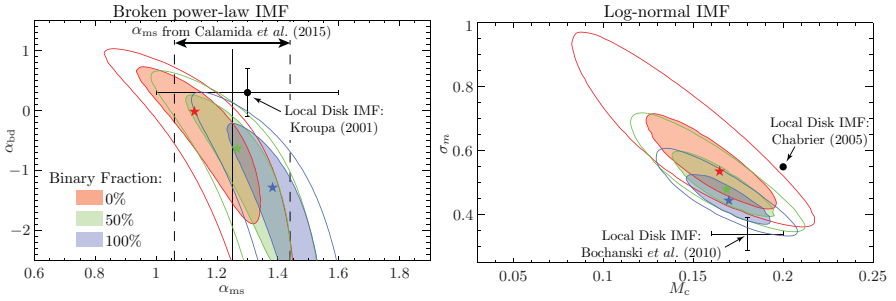

Figure 2. Left: 1σ and 2σ contours of the main sequence, $\alpha_{\rm ms}$, and brown dwarf, $\alpha_{\rm bd}$, IMF slopes. Colours correspond to varying binary fraction. The Kroupa (2001) IMF is the black point. Vertical lines show the $\alpha_{\rm ms}$ measured in the bulge by Calamida *et al.* (2015). Right: Similar for log-normal IMF. Local values are shown in black. Adapted from Wegg *et al.* (2017).

et al. (2017) displays the expected asymptotic behaviour at long timescales therefore it is likely that long timescale events were underestimated or missed in the sample of Wyrzykowski *et al.* (2015). We show in red in the left hand panel of Fig. 2 the range of power-law IMFs consistent with the data.

As is often the case in IMF determinations treatment of binaries are important. The resolution limit is approximately $R_E \sim 2$ a.u.. Wider seperated binaries are resolved into their components, while for closer binaries the total systemic mass is measured. We show binary fractions of 50 and 100% as green and blue respectively in Fig. 2.

We also considered log-normal IMFs: $dN/d\log M \propto \exp\left\{-(\log M - \log M_c)^2/2\sigma_m^2\right\}$. We show in the right hand panel of Fig. 2 the range of log-normal IMFs consistent with the same sample.

For the broken power-law IMF, we find slopes in the main sequence $\alpha_{\rm ms} = 1.31 \pm 0.10|_{\rm stat} \pm 0.10|_{\rm sys}$ and brown dwarf region $\alpha_{\rm bd} = -0.7 \pm 0.9|_{\rm stat} \pm 0.8|_{\rm sys}$ where we use a fiducial 50% binary fraction, and the systematic uncertainty covers the range of binary fractions $0 - 100\%$. Similarly for a log-normal IMF we conclude $M_c = (0.17 \pm 0.02|_{\rm stat} \pm 0.01|_{\rm sys})M_\odot$ and $\sigma_m = 0.49 \pm 0.07|_{\rm stat} \pm 0.06|_{\rm sys}$.

For both IMF parameterisations Fig. 2 suggests that the measured IMFs have slightly lower average mass than the canonical Kroupa or Chabrier values (e.g. $\sim 0.03M_\odot$ lower than Chabrier). However the differences are small compared to the error budget of local determinations and the changes induced by varying the binary fraction. We therefore conclude that the IMF in the inner Galaxy is indistinguishable from that measured in the local disk.

The P17 model predicts that the lenses have mean galactocentric radius of 2.0 kpc. The PDMF measured from the timescale distribution therefore probes the IMF in the inner Galaxy. The stars here formed on a much shorter timescale than the local disk: they are mostly α-enhanced with a formation timescale ~ 0.5 Gyr (Matteucci 2014). They are also significantly older: most bulge stars are ~ 10 Gyr old (Bensby *et al.* 2017). The consistency of the IMF between the inner MW measured here and the local disk therefore places stringent constraints on star formation models where the IMF varies according to the properties of the parent molecular gas cloud (see e.g. Guszejnov *et al.* 2017).

3. Stellar vs Dark Matter in the Bulge: A Core in the Dark Matter?

The dynamical models of the bulge in P17 used red clump stars (RCGs) as tracers of the MW's structure and therefore used a mass-to-clump ratio analogous to mass-to-light in external galaxies. P17 used $(1000 \pm 100)M_\odot$/RCG but this required assumptions about

https://doi.org/10.1017/S1743921317007542 Published online by Cambridge University Press

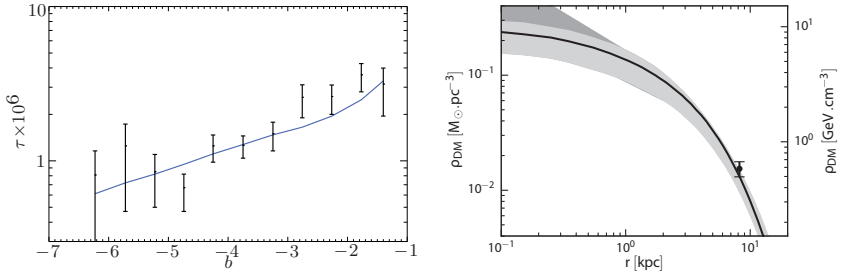

Figure 3. Left: The microlensing optical depth of the dynamical model from P17 compared with the optical depths measured by Sumi & Penny (2016). Adapted from Wegg *et al.* (2017). Right: The dark matter profiles found consistent with the data by P17. The data point is from Piffl *et al.* (2014). Figure taken from P17.

the mass of low mass stars and remnants. Microlensing constrains these and computing the mass-to-clump from the IMFs measured here gives $(960 \pm 100) M_\odot$/RCG.

Moreover, as shown in Fig. 3, the P17 model correctly predicts the microlensing optical depth. Because only stellar mass is able to microlense, the optical depth is a weighted measurement of the stellar surface density towards the bulge. The correct prediction of the optical depth therefore indicates that the stellar and dark matter contributions to the well constrained dynamical mass in the bulge are correct. The resultant dark matter fraction in the inner Galaxy is low and the disk nearly maximal (Wegg *et al.* 2016).

These results therefore strengthen the argument made in P17 that the dark matter fraction in the Bulge is low, which to be reconciled with the circular velocity and dark matter estimates locally requires a core (or shallow cusp with slope < 0.6) in the MW's dark matter halo (also independently argued by Cole & Binney 2017). The dark matter profiles found consistent with the data by P17 are shown Fig. 3.

References

Bastian, N., Covey, K. R., & Meyer, M. R. 2010, *ARAA*, 48, 339
Bensby, T., Feltzing, S., Gould, A., *et al.* 2017, *eprint arXiv:1702.02971*,
Bochanski, J. J., Hawley, S. L., Covey, K. R., *et al.* 2010, *AJ*, 139, 2679
Calamida, A., Sahu, K. C., Casertano, S., *et al.* 2015, *ApJ*, 810, 8
Calchi Novati, S., De Luca, F., Jetzer, P., Mancini, L., & Scarpetta, G. 2008, *A&A*, 480, 723
Chabrier, G. 2005, in The IMF 50 Years Later (Dordrecht: Springer Netherlands), 41
Cole, D. R. & Binney, J. 2017, *MNRAS*, 465, 798
Guszejnov, D., Hopkins, P. F., & Ma, X. 2017, *eprint arXiv:1702.04431*
Kroupa, P. 2001, *MNRAS*, 322, 231
Kunder, A., Koch, A., Michael Rich, R., *et al.* 2012, *AJ*, 143, 57
Matteucci, F. 2014, Volume 37 Saas-Fee Advanced Course (Springer Berlin Heidelberg), 145
Mróz, P., Udalski, A., Skowron, J., *et al.* 2017, *Nature*, 65, 1
Ness, M., Freeman, K., Athanassoula, E., *et al.* 2013, *MNRAS*, 432, 2092
Piffl, T., Binney, J., McMillan, P. J., *et al.* 2014, *MNRAS*, 445, 3133
Portail, M., Gerhard, O., Wegg, C., & Ness, M. 2017, *MNRAS*, 465, 1621 (P17)
Sumi, T. & Penny, M. T. 2016, *ApJ*, 827, 139
van Dokkum, P. G. & Conroy, C. 2012, *ApJ*, 760, 70
Wegg, C. & Gerhard, O. 2013, *MNRAS*, 435, 1874
Wegg, C., Gerhard, O., & Portail, M. 2015, *MNRAS*, 450, 4050
—. 2016, *MNRAS*, 463, 557
—. 2017, *ApJ*, 843, L5
Wyrzykowski, Ł., Rynkiewicz, A. E., Skowron, J., *et al.* 2015, *ApJS*, 216, 12

https://doi.org/10.1017/S1743921317007542 Published online by Cambridge University Press